Configuration dependence of deformation in ^{183}Au

P. Joshi,[1,2] A. Kumar,[1] G. Mukherjee,[2] R. P. Singh,[2] S. Muralithar,[2] U. Garg,[3] R. K. Bhowmik,[2] and I. M. Govil[1]
[1]*Department of Physics, Panjab University, Chandigarh 160 014, India*
[2]*Nuclear Science Centre, Post Box 10502, New Delhi 110 067, India*
[3]*Department of Physics, University of Notre Dame, Indiana 46556*
(Received 29 April 2002; published 23 October 2002)

The nucleus ^{183}Au was studied via lifetime measurements using the Doppler shift recoil distance method. The reaction used was ^{159}Tb(^{28}Si,4n)^{183}Au at a beam energy of 140 MeV. Transition probabilities were measured for the levels of two important bands based on $i_{13/2}$ and $h_{9/2}$ intruder configurations. The quadrupole moments extracted from measured lifetimes are ~24% larger for the $i_{13/2}$ band when compared with the $h_{9/2}$ band. The total Routhian surface calculations have been carried out using the cranked Hartree-Fock-Bogoliubov model. The calculations also support a larger deformation for the $i_{13/2}$ configuration as compared to the $h_{9/2}$ configuration.

DOI: 10.1103/PhysRevC.66.044306 PACS number(s): 21.10.Tg, 21.10.Ky, 27.70.+q

I. INTRODUCTION

The spectroscopic studies in the light Au isotopes ($A=181-187$) [1–3] have shown bands built on two low Ω ($=1/2$) deformed configurations coming from $h_{9/2}$ and $i_{13/2}$ orbitals. The $h_{9/2}$ configuration comes closer to the proton Fermi level for the lighter Au isotopes. This deformed $h_{9/2}$ configuration has been understood to be responsible for the higher prolate deformed ground state in the $A\leqslant 187$ isotopes, while the heavier ones ($A>187$) have a less deformed oblate ground state ($\beta\sim -0.15$) arising from $h_{11/2}$ configuration [4–7]. The $i_{13/2}$ level is always at a higher excitation energy when compared to the $h_{9/2}$ level. The different excitations of these two intruder orbitals with respect to the proton Fermi level are believed to influence their respective shape driving tendencies. The levels located higher in the excitation with respect to the Fermi surface are like particle states that drive the nucleus towards larger deformation, while the opposite is true for the hole like levels. The excitation energy of the $i_{13/2}$ level in the nucleus ^{183}Au is higher as compared to the Fermi level and this acts almost like a particle state thus driving the nucleus towards a larger deformation. The $h_{9/2}$ state being close to the Fermi surface would therefore prefer a lower deformation. In addition, the $i_{13/2}$ particle state, which belongs to the higher oscillator shell ($N=6$) has a larger value of $\langle r^2\rangle$ and thus is intrinsically supposed to be associated with a larger quadrupole moment. Since the transition probabilities for the $E2$ transitions give directly the quadrupole moment hence the deformation of the nucleus, we have performed lifetime measurements in the levels comprising the $E2$ sequences built on the $h_{9/2}$ and $i_{13/2}$ configurations in the ^{183}Au nucleus. The primary aim has been to investigate the effect of the different deformation driving tendencies of these two intruder configurations.

II. EXPERIMENTAL DETAILS AND DATA ANALYSIS

Lifetimes were measured in the ^{183}Au nucleus using the recoil distance Doppler shift technique. The reaction used for the experiment was ^{159}Tb(^{28}Si,4n)^{183}Au. A 140-MeV ^{28}Si beam was delivered by the 15UD pelletron at Nuclear Science Centre (NSC), New Delhi, and the NSC Plunger device [8] was employed for these measurements. A self-supporting target of ^{159}Tb(1 mg/cm^2) was stretched on the target stretcher cone while an 8-mg/cm^2-thick gold foil was stretched and used as the stopper. The distance between the target and the stopper was calibrated by the capacitance method [9]. The minimum distance between the target and the stopper was found to be 10 μm from the capacitance extrapolation curve. A gamma detector array (GDA) comprised of 12 Compton suppressed HPGe detectors (each of 23% efficiency) was used in conjunction with a 14-element BGO multiplicity filter.The HPGe detectors were arranged in a ring of four each at an angle of 144°, 98° and 50° angles, respectively, with respect to beam direction. Data from the HPGe detectors were acquired in the singles as well as in the gamma-gamma coincidence mode. However, since the intensity in the coincidence data was insufficient, the data was analyzed with the singles keeping the multiplicity gate condition ($M\geqslant 2$) which helped in suppressing the background γ rays coming from the low multiplicity processes like Coulomb excitation and radioactivity. Data were acquired for 18 target to stopper distances from 10 to 606 μm and those from detectors at each angle was gain matched in the software and added together. The average experimentally determined velocity of the ^{183}Au nuclei from the Doppler shifts of the known transitions was $v/c=0.0145$. This value has been used for the lifetime analysis of the data. The analysis of the data was performed using the computer program LIFETIME [10]. This program fits the appropriate decay curves to the experimental data and includes the effect of the side feeding corrections to the decay intensity. However, since the side feeding intensities were low as compared to the main band feeding, it will not affect the values of our lifetime measurements appreciably. In addition, the corrections are also incorporated due to the velocity dependent solid angle and the nuclear alignment attenuation. The error analysis was performed through the routine MINUIT [11] of the program LIFETIME. It determines the errors which are the increament in the value of the parameter corresponding to the unit increment in the value of the normalized χ^2 on both sides of the minimum.

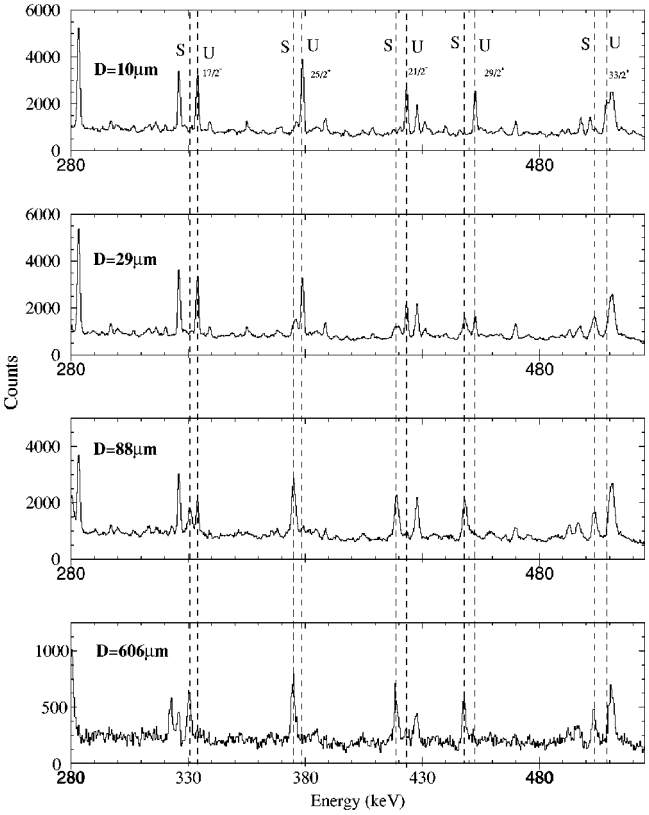

FIG. 1. The shifted (S) and unshifted (U) peaks at various target to stopper distances for ^{183}Au nucleus.

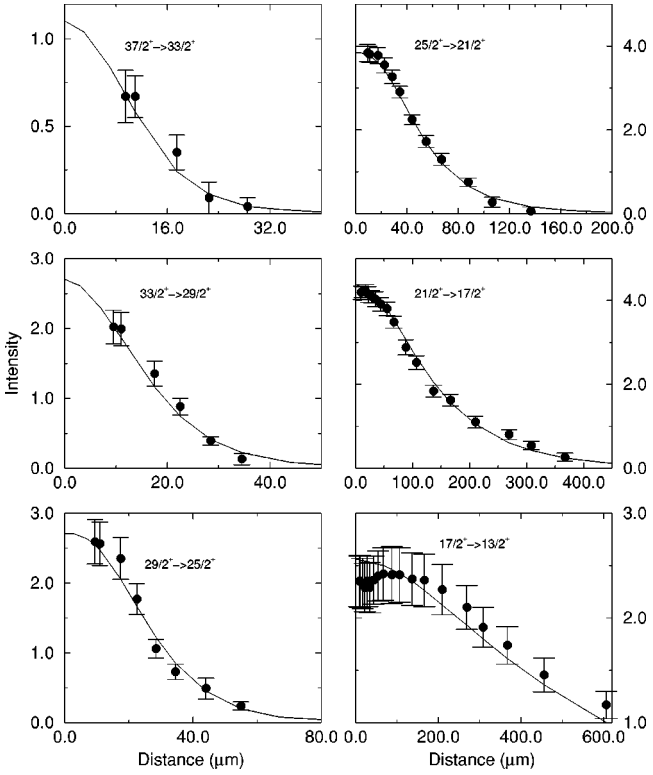

FIG. 2. The decay curves for the transitions of positive parity $i_{13/2}$ band in ^{183}Au nucleus.

III. RESULT AND DISCUSSION

A. Experimental results

Figure 1 shows the spectra for four target to stopper distances. The shifted (S) and the unshifted (U) peaks for different transitions are clearly visible in the spectrum. The areas of these shifted and unshifted peaks were efficiency corrected to get the intensity values. The decay curves for the various transitions belonging to the $i_{13/2}$ and $h_{9/2}$ bands are shown in Figs. 2 and 3, respectively. The lifetimes fitted from these curves were used to calculate the reduced transition probabilities $B(E2)$ according to the following relation:

$$B(E2)=(0.08156)/[E_\gamma^5\tau(1+\alpha_\tau)]e^2b^2, \qquad (1)$$

where E_γ is the gamma ray energy in MeV, τ is the lifetime in ps, α_τ is the total conversion coefficient. The measured lifetime values and the reduced transition probabilities are shown in Tables I and II for the $i_{13/2}$ and the $h_{9/2}$ bands, respectively. These measured $B(E2)$ values were used for calculating the transition quadrupole moments for getting an idea about the shape of the nucleus. The extracted quadrupole moments for both these bands are plotted in Fig. 4 as a function of the rotational frequency. The average value of the quadrupole moments is $\sim$24% higher for the $i_{13/2}$ band than the $h_{9/2}$ band which indicates a larger deformation of the $i_{13/2}$ band as compared to the $h_{9/2}$ band.

B. Theoretical calculations

To investigate the shapes associated with these configurations, we have performed total Routhian surface (TRS) calculations using the microscopic-macroscopic approach. The Routhians were calculated using the cranked Hartree-Fock-Bogoliubov procedure [12,13]. A rotating Woods-Saxon mean field potential [14,15] along with the monopole pairing interaction was used for these calculations. The values of the pairing term Δ and the chemical potential λ for the ground state were determined by solving the BCS self-consistent equations [16]. The total Routhian calculations were used for determining the microscopic corrections to the macroscopic energy using the Strutinsky procedure [14]. These total Routhian surfaces (TRS's) were calculated for the positive signature of the positive parity as well as negative parity configurations for a set of points in the $\beta-\gamma$ mesh. A minimization in the β_4 degree of freedom was performed for each mesh point. The equienergy contours for these two configurations are shown in Fig. 5 for a rotational frequency of $\hbar\omega=0.20$ MeV being the average energy of the measurements.

The TRS plot for the positive parity configuration shows a minimum at $\beta=0.28$ and it is associated with a triaxiality $\gamma=+3°$. The negative parity configuration, on the other hand, shows a smaller deformation $\beta=0.24$ and triaxiality $\gamma=-1°$. Thus these theoretical TRS calculations predict that the positive parity configuration has a deformation $\sim$17% higher than the negative parity configuration.

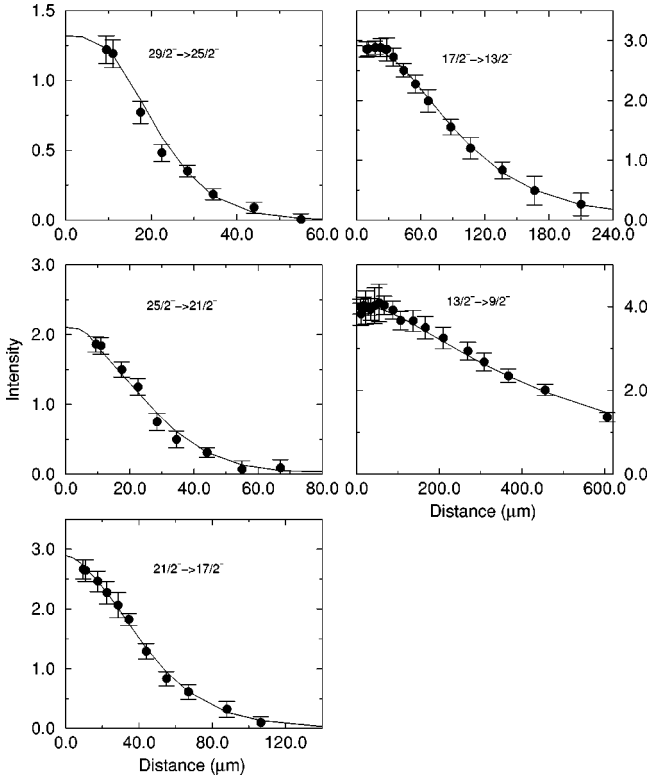

FIG. 3. The decay curves for the transitions of negative parity $h_{9/2}$ band in ^{183}Au nucleus.

As mentioned earlier, the experimental transition quadrupole moment Q_t values for the $i_{13/2}$ band are also found to be 24% larger compared to the $h_{9/2}$ band. The deformation parameter β was extracted from the experimental Q_t values using a linear expansion of the Q_t in terms of β for an axially deformed shape of the nucleus ($\gamma=0°$) using the following relation:

$$Q_t=\frac{3}{\sqrt{5\pi}}ZeR_0^2\beta, \tag{2}$$

where $R_0=1.2A^{1/3}$. These values of β which are shown in Fig. 4 are 24% larger for the $i_{13/2}$ positive parity band as compared to the $h_{9/2}$ negative parity band.

The increase in the deformation for the $i_{13/2}$ band can be attributed to the larger deformation-driving property of this highly down-sloping intruder configuration. The energy of any quasiproton orbit E_{qp}, at any deformation β is given by [17]

$$E(\beta)_{qp}=\sqrt{[(e_\nu(\beta)-\lambda)^2+\Delta_p^2]} \tag{3}$$

where λ and Δ_p are the energies of Fermi level and the pair gap, respectively, and $e_\nu(\beta)$ is the energy of the proton single particle or hole state as a function of deformation β. A level is defined as particle (hole) if its energy $[e_\nu(\beta)]$ is higher (lower) than the Fermi level. It is seen from the above equation that for the negative slope of e_ν against β, of the particle (hole) state, the corresponding quasiparticle energy $E(\beta)_{qp}$ would have a negative (positive) slope. Thus the particle states are prolate driving while the hole states would show the opposite effect.

Figure 6 shows quasiproton Routhians $E(\beta)_{qp}$ for positive as well as negative parity configurations plotted against

TABLE I. Lifetimes and the $B(E2)$ values for the positive parity $i_{13/2}$ band in ^{183}Au.

Energy (keV)	Transition $(I_i^\pi \to I_f^\pi)$	Lifetime (ps)	$B(E2)$ (e^2b^2)
164	$\frac{17}{2}^+ \to \frac{13}{2}^+$	$222\pm{}^{8}_{9}$	$1.75\pm{}^{0.07}_{0.06}$
283	$\frac{21}{2}^+ \to \frac{17}{2}^+$	$24.2\pm{}^{0.5}_{0.5}$	$1.65\pm{}^{0.03}_{0.03}$
379	$\frac{25}{2}^+ \to \frac{21}{2}^+$	$5.86\pm{}^{0.19}_{0.16}$	$1.68\pm{}^{0.05}_{0.05}$
453	$\frac{29}{2}^+ \to \frac{25}{2}^+$	$2.71\pm{}^{0.14}_{0.13}$	$1.52\pm{}^{0.08}_{0.07}$
510	$\frac{33}{2}^+ \to \frac{29}{2}^+$	$1.58^{+0.15}_{-0.18}$	$1.48\pm{}^{0.19}_{0.13}$
558	$\frac{37}{2}^+ \to \frac{33}{2}^+$	<0.97	>1.54

TABLE II. Lifetimes and the $B(E2)$ values for the negative parity $h_{9/2}$ band in ^{183}Au.

Energy (keV)	Transition $I_i^\pi \to I_f^\pi$	Lifetime (ps)	$B(E2)$ (e^2b^2)
219	$\frac{13}{2}^- \to \frac{9}{2}^-$	$116\pm{}^{6}_{6}$	$1.08\pm{}^{0.06}_{0.06}$
334	$\frac{17}{2}^- \to \frac{13}{2}^-$	$14.6\pm{}^{1.3}_{1.2}$	$1.25\pm{}^{0.11}_{0.10}$
424	$\frac{21}{2}^- \to \frac{17}{2}^-$	$5.60\pm{}^{0.36}_{0.51}$	$1.03\pm{}^{0.10}_{0.06}$
503	$\frac{25}{2}^- \to \frac{21}{2}^-$	$2.54\pm{}^{0.24}_{0.26}$	$1.00\pm{}^{0.11}_{0.08}$
572	$\frac{29}{2}^- \to \frac{25}{2}^-$	<1.22	>1.06

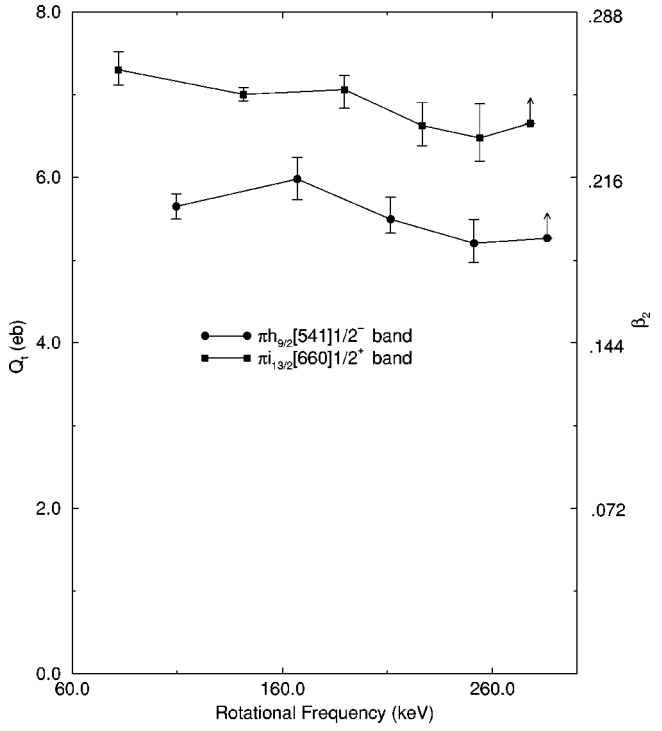

FIG. 4. The transition quadrupole moments extracted from the measured transition probabilities for the $i_{13/2}$ and $h_{9/2}$ bands in ^{183}Au nucleus. The solid lines are the guide to the eye.

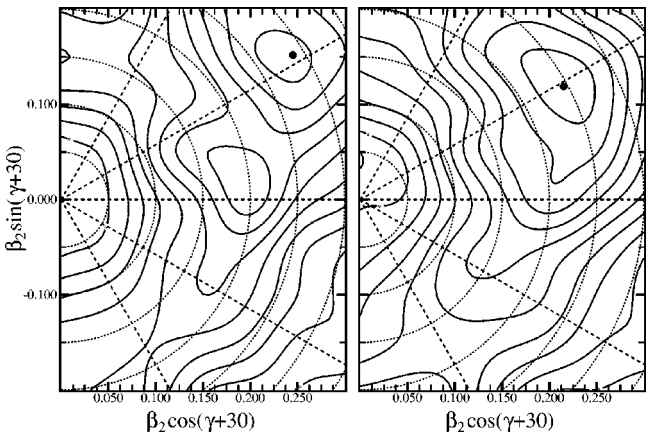

FIG. 5. The TRS plots for the positive parity and positive signature (left) as well as the negative parity and positive signature (right) configurations. Both the plots correspond to a rotational frequency of $\hbar\omega = 0.20$ MeV.

the deformation parameter β for the nucleus ^{183}Au ($Z = 79$), at a rotation of $\hbar\omega = 0.2$ MeV. The level coming from $i_{13/2}$ configuration, which is predominantly a particle state, comes down in energy as a function of deformation and hence shows a deformation driving tendency. The negative parity level coming from the $h_{9/2}$ configuration rises up in energy as a function of increasing deformation therefore it does not prefer a larger deformation. The measurements of the transition quadrupole moments by Muller *et al.* [18] in the nucleus ^{179}Ir have shown that the deformation of the positive parity $i_{13/2}$ band is $\sim$30% larger than the $h_{9/2}$ band. Since the energy of the proton Fermi level in Ir ($Z = 77$) is lower than Au ($Z = 79$), the excitation of the $i_{13/2}$ orbit with respect to the Fermi surface would be even large in Ir nuclei therby making it more deformation driving. However, as one continues towards the lower-Z nuclei, the energy of the proton Fermi level goes further down and the excitation of the $h_{9/2}$ configuration above the Fermi level starts increasing, and it becomes a predominantly particle state in ($Z = 73$) tantalum nuclei which drives the nuclear shape towards a larger deformation [8,19,20].

IV. SUMMARY

Lifetimes have been measured for levels of the $i_{13/2}$ and $h_{9/2}$ bands in ^{183}Au nucleus using the Doppler shift recoil distance technique. These lifetimes were used to extract the $B(E2)$ values and the transition quadrupole moments (Q_t). The extracted Q_t's indicate a larger deformation for the $i_{13/2}$ band as compared to the $h_{9/2}$ band. The TRS calculations also predict $\sim$15% larger value of β_2 for the $i_{13/2}$ configuration as compared to the $h_{9/2}$ configuration. The energies of the $i_{13/2}$ as well as the $h_{9/2}$ quasiprotons have been calculated as a function of deformation β_2, using the cranked Hartree-Fock-Bogoliubov (CHFB) calculations. The higher excitation of the proton $i_{13/2}$ configuration above the Fermi level allows it to drive the nucleus towards higher deformation while the $h_{9/2}$ level located just below the Fermi level prefers a lower deformation.

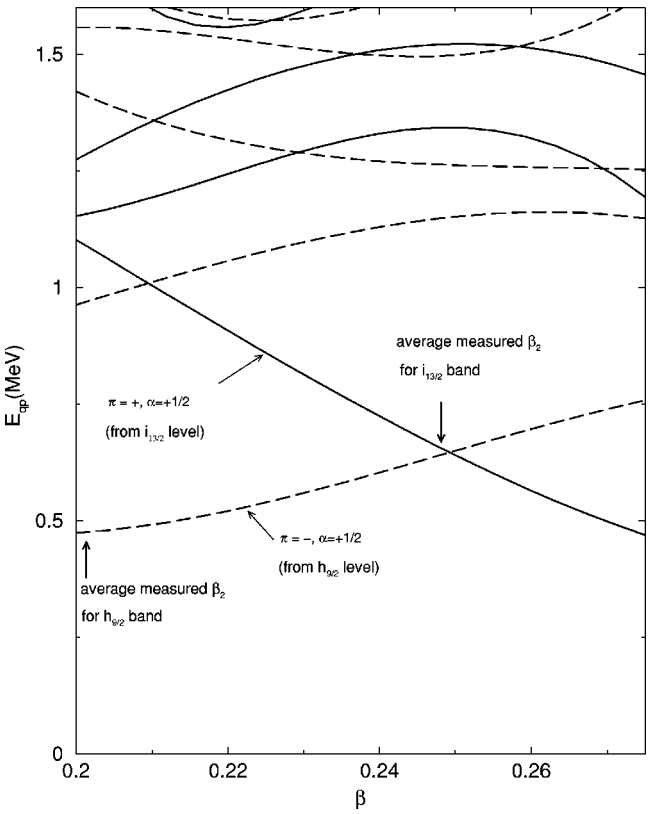

FIG. 6. The quasiproton Routhians for positive parity positive signature (solid line) as well as negative parity positive signature (dashed line), plotted against deformation β at a rotational frequency of $\hbar\omega = 0.20$ MeV for ^{183}Au nucleus.

[1] W.F. Mueller *et al.*, Phys. Rev. C **59**, 2009 (1999).
[2] A.J. Larbee *et al.*, Phys. Lett. **169B**, 21 (1986).
[3] D. Rupnik *et al.*, Phys. Rev. C **58**, 771 (1998).
[4] K. Wallmeroth *et al.*, Nucl. Phys. **A493**, 224 (1989).
[5] M.A. Deleplanque *et al.*, Nucl. Phys. **A249**, 366 (1975).
[6] V. Berg *et al.*, Nucl. Phys. **A244**, 462 (1975).
[7] P. Tjom *et al.*, Nucl. Phys. **A231**, 397 (1976).
[8] P. Joshi *et al.*, Phys. Rev. C **60**, 034311 (1999).
[9] T.K. Alexander and A. Bell, Nucl. Instrum. Methods **81**, 22 (1970).
[10] J. C. Wells *et al.*, ORNL/TM-9105, 1985.
[11] F. James and M. Roos, Comput. Phys. Commun. **10**, 343 (1975).
[12] P. Ring and P. Schuck, *The Nuclear Many Body Problem* (Springer-Verlag, Berlin, 1980), p. 244.
[13] W. Nazarewicz, M.A. Riely, and J.D. Garrett, Nucl. Phys. **A512**, 61 (1990).
[14] T.R. Werner and J. Dudek, At. Data Nucl. Data Tables **59**, 1 (1995).
[15] T.R. Werner and J. Dudek, At. Data Nucl. Data Tables **50**, 179

(1992).
[16] S. G. Nilsson and I. Ragnarsson, *Shapes and Shells in Nuclear Structure* (Cambridge University Press, Cambridge, England, 1995), p. 290.
[17] S. G. Nilsson and I. Ragnarsson, *Shapes and Shells in Nuclear Structure* (Ref. [16]), p. 317.
[18] D. Muller *et al.*, Phys. Lett. B **332**, 265 (1994).
[19] L.L. Riedinger *et al.*, Nucl. Phys. **A520**, 287c (1990).
[20] P. Joshi *et al.*, Phys. Rev. C **64**, 034303 (2001).